GSA Data Repository 2019XXX

Preservation of organic carbon during active fluvial transport and particle abrasion

Joel S. Scheingross[1,2*], N. Hovius[1,3], M. Dellinger[4], R.G. Hilton[4], M. Repasch[1,3], D. Sachse[1], D.R. Gröcke[5], A.Vieth-Hillebrand[1], and J.M. Turowski[1]

[1]*GFZ German Research Centre for Geosciences, Potsdam, Germany*
[2]*Dept. of Geological Sciences and Engineering, University of Nevada, Reno, USA*
[3]*Institute of Geosciences, University of Potsdam, Germany*
[4]*Dept. of Geography, Durham University, UK*
[5]*Dept. of Earth Sciences, Durham University, UK*
**jscheingross@unr.edu*

Data Repository Text

1. Additional experimental materials and methods

We used stainless steel flume and control tanks to minimize contamination from organic material. Flumes were annular (35 cm tall with 25 and 15 cm outer and inner radii, respectively) while control tanks were cylindrical (25 cm tall by 33 cm in diameter). In flumes, hydraulic roughness was provided by placing a removable, 3.2 mm thick stainless steel sheet cut into a wave pattern on the flume floor (Figure 1B). All experiments began with ~20-30 h of clear water flow before adding sediment, this allowed assessment of contamination from flume and control tanks via monitoring changes in the dissolved load. To ensure a well-mixed system, control experiments were hand-stirred for ~10 seconds, ~5 times per week. Flume and control experiments used 29.3 ± 0.4 and 16.0 ± 0.2 L of water, respectively (Table DR2). We measured water loss due to evaporation and sampling via point gage measurements of the flume and control water levels at the start and end of each experiment, using the difference between measurements and the tank geometry to estimate the total water volume loss (Table DR2).

2. Flow velocity and sediment transport

In our flume experiments, flow was driven by rotating paddles that spun at 58±2.5 revolutions per minute (RPM). We measured downstream flow velocity in the flumes using an OTT C2 propeller-style flow meter placed in the center of the channel and oriented perpendicular to the main flow direction (Table DR1). All flow measurements were made in triplicate and averaged over 60 s. Depth-averaged flow velocities, U_{fluid}, for conditions in our experiment ranged from 0.24 to 0.26 m/s (Table DR1), and we use a flow velocity of 0.25 m/s for all sediment transport calculations.

We make separate estimates of particle transport distance for suspended sediment and bedload. In the downstream direction, suspended sediment is transported at the fluid velocity (McLean, 1992; Garcia, 2008), such that the suspended sediment transport distance, x_{susp}, can be approximated as

$$x_{susp} = U_{fluid} t \ , \qquad \text{(DR1)}$$

where t is time. Data compilations show bedload saltation velocity tends to be ~60-80% of the fluid velocity (Chatanantavet et al., 2013); we estimate bedload transport distance, $x_{bedload}$, as

$$x_{bedload} = 0.7 x_{susp} \quad . \tag{DR2}$$

We mark the transition from bedload to suspended load transport using the ratio between fluid shear velocity, u_* (a proxy for fluid turbulence), and still water particle terminal settling velocity, w_s. Estimates for the onset of suspension vary range for $u_*/w_s > 0.2 – 2$ (Chanson, 2004), and $u_*/w_s > 1$ is often used as an order of magnitude estimate (Bagnold, 1966). We estimate particle settling velocity following Dietrich (1982), and estimate shear velocity by re-arranging a standard channel flow resistance equation (Garcia, 2008)

$$u_* = \frac{U}{8.1(H / k_s)^{1/6}} \quad , \tag{DR3}$$

where H = 23 cm is the flume flow depth and k_s is a roughness length scale which we set equal to the 3.2 mm relief of the wave-cut sheet placed on the flume floor. Following this analysis, the threshold for suspension occurs for grains finer than ~160 μm diameter, resulting in sediment transport primarily in suspension for all but two of our main experiments (Table DR2).

3. Sediment collection and preparation prior to experiments

We collected Jurassic Posidonia shale and Miocene Lusatian lignite from fresh outcrops exposed at open-pit mines near Dotternhausen, Germany and Cottbus, Germany, respectively (Schreck and Glasser, 1998; Rohl et al., 2001). Sediment from Lookout Creek, USA (Smith, 2013) and Rio Bermejo, Argentina (Scheingross et al., 2018) was collected with a clean trowel from channel deposits exposed during low flow. Visual observation showed Lookout Creek and Rio Bermejo samples included fragments of leaf litter and other discrete organic particles. These samples are likely to also have mineral-associated biospheric organic matter due to the presence of fine grains, but we made no effort to distinguish if and how organic matter was bound to sediment, instead focusing on the bulk POC behavior.

All samples were oven-dried at temperatures between 40-60 ºC upon return to the lab. After drying, we crushed lignite and shale samples, wet-sieved samples to distinct grain size fractions, re-oven dried sediment, and introduced sediment into the experiments. Sieving of sediments into different size fractions allowed examination of the role of particle abrasion. Larger grain sizes have higher kinetic energy of impact, producing more abrasion (Sklar and Dietrich, 2004), while grains with less than ~200 μm diameter in our experiment had viscous damping of impacts, limiting abrasion (Joseph et al., 2001; Scheingross et al., 2014).

4. Sample collection, processing and analytical techniques

Our water and sediment sampling frequency represents a tradeoff between high frequency measurements and limiting disturbance to the experiment. We chose water sampling frequency based on preliminary measurements from our pilot experiments (Data Repository Section 9) in order to capture major trends while minimizing the total water extracted, and limited sediment sampling to only before and after the experiment in order to obtain large sample volumes without the need to drain water from the experiments.

We used a high-density polyethylene (HDPE) syringe rinsed in de-ionized water to collect water samples from the surface of the flume and control tanks for analysis, and filtered water with single-use 0.22 μm polyethersulphone (PES) filters. At the time of water sampling, we measured pH, conductivity, dissolved oxygen, and water temperature in both flume and

control tanks with a multiprobe (Table DR5). We stored samples for DOC analysis in combusted glass vials and all other samples in HDPE bottles triple-rinsed with de-ionized water. Samples for rhenium and cation analysis were acidified with 32% nitric acid immediately after sample collection. All water samples were refrigerated from the time of collection until sample analysis.

We measured DOC concentration by liquid-chromatography organic carbon detection (LC-OCD). Phosphate buffer (pH 6.85; 2.5 g KH_2PO_4, 1.5 g Na_2HPO_4) was used as mobile phase with a flow of 1.1 ml/min. Quantification of DOC was done by IR-detection of released CO_2 after UV photooxidation (λ = 185 nm) in a Gräntzel thin-film reactor. Replicate measurements of DOC consistently yielded error less than 25% of the measurement value (Figure DR3 and Table DR4) and we conservatively apply an error of 25% to all measurements, and propagate this 25% error in f_{DOC} calculations (Eq. 2).

Cations were measured with a Varian 720 inductively coupled plasma optical emission spectrometer (ICP-OES) at the Helmholtz Laboratory for the Geochemistry of the Earth Surface at GFZ Potsdam following Schuessler et al. (2016) (Table DR6). We used SLRS-5 (Saint-Laurent River Surface, National Research Council - Conseil National de Recherches Canada) and USGS M212 and T187 as external standards and measured an internal standard (GFZ-RW1) every 10 samples to correct for instrument drift. We report measurement error based on calibration uncertainties (Table DR7). We used a Dionex ICS1100 Ion Chromatograph to measure anion concentrations, using USGS standards M206, M208, and M212 as external standards and for quality control, we report standard deviation of triplicate measurements as an assessment of sample uncertainty (Tables DR6 and DR7). We used the inorganic dissolved data to estimate HCO_3^- using a charge balance (excluding Si), and summed all anions and cations to estimate total dissolved solids (TDS). Propagating uncertainties gives TDS error of 2-7% (Table DR7).

Dissolved rhenium concentration was determined by direct calibration against a set of seven standards with varying Re abundances and similar matrixes to river water, using quadrupole inductively coupled plasma mass spectrometry (Q-ICP-MS, Agilent Technologies 7900). Standards and samples were doped with a known concentration of internal standard Tb and Bi to correct for instrumental drift. Accuracy and precision of the measurements was assessed by repeated measurements of riverine standard reference materials SLRS-5 and SLRS-6. The standards confirmed better than 5% accuracy and precision, and we propagate 5% uncertainty from these measurements in calculations of f_{Re} (Eq. 3).

Total water collection for sample analysis in experiments was typically less than ~0.8 - 1 L in each of the flume and control tanks. This water was not replaced, except in experiments 4 – 6 (Table DR2) where we added an additional 700 ml of 1:10 tap:de-ionized water to both the flume and control tanks after ~18 days of run time to offset water extraction. In experiments 7, 9, 10, 11, and 14 (Table DR2) we also sampled an additional 1 L of water approximately half way through the experiment for separate analyses, and immediately replaced the sampled water with 1:10 tap:de-ionized water. The dilution factor from water extraction did not exceed ~6%, significantly less than our conservative estimate of 25% error on DOC measurements. For simplicity, we assume error associated with water extraction and addition is subsumed in our estimates of DOC error and do not include error associated with water extraction in our uncertainty estimates of f_{DOC} (Eq. 2).

Initial sediment samples reflecting POC composition at the start of the experiment were collected prior to sediment introduction in the flume and control tanks. We filtered flume and control water through single-use 0.22 μm PES filters at the end of experiments to retrieve sediment. In select cases we allowed sediment to settle for >12 h and decanted a portion of the clear water before either filtering or allowing the remaining water to evaporate in a drying oven between 40-50 ºC. After collection, sediment was oven-dried between 40-50 ºC for >24 h and stored in combusted glass vials.

Dried sediment samples were split into separate aliquots for grain size measurements at the GFZ Sed Lab and geochemical analysis at Durham University. In all experiments aliquots for grain size analysis were placed in a sodium pyrophosphate dispersion agent for >24 h to break down aggregates before running samples through a laser diffraction particle size analyzer (Retsch/Horiba LA950) capable of measuring particles between 0.1 and 2500 μm in 92 logarithmically spaced bins. Counts were converted to volume percent applying the Mie scattering theory with a refraction index of 1.55 and an absorption index of 1.33, and we calculated particle size distribution based on the median of 10 successive measurements. Replicate analysis of select samples showed variation in median grain size (D_{50}) up to ~15%. We conservatively apply 15% uncertainty to all laser diffraction measurements, and propagate this error in estimates of ΔD_{50} (Figure 2A).

Large grain sizes in Experiments 6 and 14 (Table DR3) led to >15% variability in laser diffraction measurements, due in part to the small sample sizes (typically <0.4 g) used for laser diffraction analysis. For all material from Experiment 14 and the starting material and ending material from the control tank in Experiment 6, we instead measured grain size distributions using a Retsch Camsizer XT (Table DR3) which can measure large sample masses (>10g) to capture sample heterogeneity. The Camsizer digitally images grains and measures grain diameter over 297 linearly spaced bins between 30 μm – 3 cm. We use the Camsizer grain diameter estimate based on the equivalent diameter of the area equivalent circle of the particle projection. Replicate analysis of select Camsizer measurements shows D_{50} variability <5%, and we propagate this 5% error in ΔD_{50} calculations (Figure 2A). Significant abrasion in the flume run of Experiment 6 produced fine grains that were below the detection limit of the Camsizer, and we report grain size estimates from laser diffraction measurements for this run (Table DR3).

For select samples, we additionally measured specific surface area (SSA) of sediments using a Micromeritics Gemini VII gas sorption analyzer. We measured the molar amount of nitrogen gas (N_2) adsorbed to the total particle surface area in 1-2 grams of bulk sample material under increasing gas pressure. For each sample, a linear adsorption isotherm was calculated using measurements at five pressure conditions and specific surface area (m^2/g dry sediment) was determined using the Brunauer, Emmett, and Teller (BET) theory (Brunauer et al., 1938).

Solid sample aliquots (~20 g) for geochemical analyses were powdered in a disc mill and decarbonated following Galy et al (2007). C_{org} and stable carbon isotope measurements were carried out using a Costech Elemental Analyser (EA) coupled via a CONFLO III to a Thermo Scientific Delta V Advantage isotope ratio mass spectrometer (IRMS) at Durham University. Measurements were normalized using internal and international standards and corrected for internal and procedural blanks (Grocke et al., 2011). Stable carbon isotope ratios are reported in

$\delta^{13}C$ notation relative to Vienna Pee Dee belemnite (VPDB). Isotopic accuracy was monitored through routine analyses of in-house standards, which were stringently calibrated against international standards (e.g., USGS 24, 40, IAEA 600, CH3, CH7): this provided a total linear range in $\delta^{13}C$ between –46‰ and +3‰. Analytical uncertainty in $\delta^{13}C$ was typically ±0.1‰ or better for replicate analyses of the international standards. Total organic carbon was obtained as part of the isotopic analysis using an internal standard (Glutamic Acid, 40.82%C). Error on calculating C_{org} using replicate analyses of the internal standard and duplicate analyses is on the order of 3% of the measured value. We propagate 3% error on C_{org} in all ΔM_c calculations.

The concentration of Re in solid samples was determined with 300 to 500 mg of powdered sample in a volume of 3 mL HF 27N and 3 mL of HNO_3 16N in PTFE beakers heated at 120°C for at least 24 h. After digestion, samples were evaporated until dry at 80°C and then re-dissolved in aqua regia in order to destroy fluorides and heated at 120°C for 24 h before being re-evaporated again. Finally, samples were re-dissolved in HCl (concentration ~1N). For samples containing refractory organic matter, the solid black residue was treated in concentrated HNO_3 16N and aqua regia for several days at temperature of 160°C in order to oxidize a maximum amount of organic matter. Rhenium was then separated from the rest of the matrix using an ion-chromatography chemical procedure modified from previously described methods (Miller et al., 2009; Chu et al., 2015). Polypropylene columns with an inner diameter of the bed area of 7.1 mm were filled with 1 mL of AG1-X8 resin (200-400 mesh) which was cleaned (30 mL of HNO_3 8N) and conditioned (5 mL of HCl 1N) before introduction in a HCl 1M medium. Before eluting the Re, elution of the rest of the matrix was done in 3 steps: (1) matrix cleaning by adding 10 mL of HCl 1N, (2) addition of 15 mL of HNO_3 0.5N, and (3) 1.5 mL of HNO_3 4N. Re was eluted with 12.5 mL of HNO_3 4N. After elution, the Re eluted fraction was evaporated at 100-120°C until completely dry. Re was re-taken into solution and concentration was measured by direct calibration as per water samples (described above).

5. Changes in water temperature, pH, and dissolved oxygen

For our experiments, flume water temperatures were typically near 24±3ºC, and motor heat caused flumes to run ~3 ºC higher than their corresponding static control tanks (Table DR5). Water pH started at ~7.5 and typically remained between 7 and 8.5, (with the exception of the lignite experiment where values decreased to ~5 to 4) (Table DR5). Except for a single outlier, dissolved oxygen levels in flume experiments always exceeded 95%. Dissolved oxygen in control experiments was typically above 90%, with the exception of the lignite experiment where values progressively decreased from ~98% to 55% (Table DR5).

6. Quantifying solid phase POC loss

Calculation of ΔM_c (Eq. 1) requires estimates of the initial and final carbon mass. We estimate $M_{c\_initial}$ as

$$M_{c\_initial} = \frac{C_{org\_initial}}{100} \times M_{sed} \quad , \qquad \text{(DR4)}$$

where $C_{org\_initial}$ and M_{sed} are the initial POC concentration (wt. %) and experiment sediment mass, respectively. To calculate M_{c_final} we correct the POC concentration measured at the end of the experiment (C_{org_final}, wt. %) for mass loss to the dissolved phase (M_{diss}) as

$$M_{c\_final} = \frac{C_{org\_final}}{100}\left[M_{sed} - M_{diss}\right] . \quad \text{(DR5)}$$

We calculate M_{diss} from the change in TDS and tank water volume (V)

$$M_{diss} = TDS_{final}V_{final} - TDS_{initial}V_{initial} , \quad \text{(DR6)}$$

where the subscripts initial and final refer to the start and end of the experiment, respectively.

The main contributors to TDS are Ca^{2+}, SO_4^{2-} and HCO_3^- (Table DR6) indicating carbonate dissolution and sulfide oxidation during the experiments. Mass loss from solids due to DOC production was negligible relative to TDS (Tables DR4 and DR6). Propagating uncertainty from TDS, C_{org}, and V results in ~4% error on ΔM_c measurements, which stem primarily from the 3% uncertainty in C_{org}. Water addition in select experiments (DR Section 3) resulted in TDS changes of up to 2%, less than the up to 7% uncertainty on TDS measurements, and, for simplicity, is not included in M_{diss} uncertainty estimates.

Despite the mass loss correction, three of the control experiments and one of the flume experiments show POC gain (ΔM_c values of 7±4% and 8±4%, Figure 2b). Gains likely reflect heterogeneity in C_{org} values within samples beyond what is accounted for in the 3% uncertainty. Small amounts of POC-enriched (e.g. macromolecular organic matter) or POC-depleted (mineral grains, quartz) phases could shift the measured C_{org} values. Small gains in POC are consistent with our general finding of less than 10% POC mass loss (ΔM_c>-10%) during experiments (Figure 2B). Future, more precise measurements of POC loss may benefit from tracking the gaseous products of oxidation such as CO_2 (e.g., Beaupre et al., 2016).

Estimates of f_{DOC} (Eq. 2) use the maximum measured mass of DOC over the experiment (M_{DOC_max}) calculated as

$$M_{DOC\_max} = DOC_{max}V_{t\_max} - DOC_{initial}V_{initial} , \quad \text{(DR7)}$$

where $DOC_{initial}$ and DOC_{max} are the initial and maximum DOC concentrations measured before and after adding sediment to the experiment, respectively, and V_{t_max} is the flume or control tank volume at the time of the maximum DOC concentration, and is estimated from a linear interpolation of $V_{initial}$ and V_{final} (Table DR2). We propagate uncertainty on DOC, V, and $M_{c\_initial}$ measurements to estimate f_{DOC} error.

7. Dissolved load geochemistry during POC_{petro} experiments

Shale experiments showed consistent behavior in the evolution of major (Ca^{2+}, SO_4^{2-}, TDS) and trace (Re) dissolved ion concentrations during the experiments. The sediment addition caused a rapid increase in major ion concentrations over a period of ~4 days, followed by a slower increase in concentration during the remaining experiment time (Figure DR4). The lignite experiment showed similar behavior to the shale experiments with initially rapid increase in Re and SO_4^2 over the first ~1 day, which slowed with time (Figure DR4). The rapid increase in dissolved concentrations following sediment addition may reflect ion-exchange between fresh sediment and a fluid that is not in equilibrium with that solid (e.g., Sayles and Mangelsdorf, 1979; Lupker et al., 2016), rapid release of solutes from defect sites (White and Brantley, 2003), and/or rapid carbonate weathering (Chou et al., 1989).

Regardless of the exact chemical process that takes places during the first 1-4 days of POC_{petro} the experiments, the rapid solute production does not well represent the processes acting in lowland rivers, where sediments have been in contact with water since prior to their erosion (e.g. in the saturated zone) and during erosion, transport and deposition. Here we seek to examine the slower production of solutes that occurs by oxidation and/or acid-hydrolysis reactions ("weathering") between the fluid and solid that occurs after the initial rapid solute production. To do this, we examine the dissolved Re/SO_4 versus Re/Na ratios over the duration of the experiments. Oxidation of sulfide minerals is expected to outpace POC_{petro} oxidation, which in turn outpaces silicate mineral acid hydrolysis (Chang and Berner, 1999). This suggests that weathering reactions should increase SO_4, Re and Na concentrations over time, but that Re/SO_4 should decrease while Re/Na increases over time. This behavior starts at around 1 and 4 days in the lignite and shale experiments, respectively, and continues for the remaining portion of the experiment (Tables DR2 and DR6, Figure DR5), consistent with a switch from ion-exchange, leaching, or rapid carbonate dissolution to "weathering" reactions. We remove Re produced in this initial period of rapid solute production from our calculation of f_{Re} (Eq. 3) by solving for M_{diss_Re} as

$$M_{\mathrm{diss\_Re}} = \mathrm{Re}_{final} V_{final} - \mathrm{Re}_{initial} V_{initial} - M_{blank} \quad \text{(DR8)}$$

where Re_{final} is the Re concentration at the end of the experiment and $Re_{initial}$ is the Re concentration after 1 and 4 days in the lignite and shale experiments, respectively. M_{blank} is a correction for Re production that occurred in blank experiments (Figure DR2, Tables DR2 and DR6). For flume experiments with D_{50}>250 μm, we set M_{blank} to 60 ng based on the 60 ng increase in rhenium in the blank experiment transporting combusted quartz sediment (which we attribute to abrasion of the stainless steel flume and/or production of Re from inclusions in the silicate mineral). Other POC_{petro} experiments had grain sizes below the threshold for viscous dampening and we set M_{blank} = 0.3 ng for flume experiments based on the increase in rhenium in the sediment-free blank experiment. We set M_{blank} = 0 g for all control experiments based on negligible increases in rhenium in control experiments (Table DR6). Finally, we calculate the initial solid load mass of Re as

$$M_{\mathrm{Re\_initial}} = \mathrm{Re}_{initial} \times M_{sed} \quad \text{(DR9)}$$

where $Re_{initial}$ is the sediment rhenium concentration at the start of the experiment.

8. Comparison with field estimates of POC loss

We seek to estimate the loss of POC_{petro} that occurs between the mountain front and coastline in the Amazon and Gages rivers. Because POC_{petro} in these basins is sourced exclusively from the river headwaters, the losses represent the total POC_{petro} loss from both in-river fluvial transport and floodplain storage. In the Amazon basin, Bouchez et al. (2010) report a decrease in C_{org_petro} from 0.26%±0.11% at the mountain front (the Rio Beni near Rurrenabaque, Bolivia) to 0.02%±0.03% in the lowland basin (the mouth of the Rio Madeira, Brazil). Using the upper limit of C_{org_petro}=0.37% at the mountain front and the mean value of C_{org_petro}=0.02% in the lowland basin, we estimate an upper bound of 95% POC_{petro} loss during lowland river transit. This estimate assumes that C_{org_petro} is not influenced by sediment input from unconstrained tributaries, which deliver ~60% of the total sediment load (Bouchez et al., 2010). To account for sediment from unconstrained tributaries, we represent POC_{petro} concentration measured at the

mouth of the Rio Madeira ($C_{org\_petro\_Madeira}$) as a mix of POC_{petro} from sediment sourced from the Rio Beni ($C_{org\_petro\_Beni\_source}$) and unconstrained tributaries ($C_{org\_petro\_unconstrained\_sources}$), i.e.,

$$C_{org\_petro\_Madiera} = 0.4(C_{org\_petro\_Beni\_source}) + 0.6(C_{org\_petro\_unconstrained\_sources}) \ . \quad \text{(DR10)}$$

Solving Eq. (DR10) for $C_{org\_petro\_Beni\_source}$ assuming the sediment from unconstrained tributaries is POC_{petro} free ($C_{org\_petro\_unconstrained\_sources} = 0$), and conservatively assuming $C_{org\_petro\_Madeira}$ varies between its mean value (0.02%) and its upper limit (0.05%), yields $0.05\% < C_{org\_petro\_Beni\_source} < 0.125\%$. We thus estimate C_{org_petro} loss using the lower limit of $C_{org\_petro} = 0.15\%$ measured at the mountain front and the upper limit of $C_{org\_petro} = 0.125\%$ in the lowland basin after 60% dilution from assumed POC_{petro} free tributaries. This yields a conservative lower estimate of POC_{petro} loss of 17%.

For the Ganges basin, C_{org_petro} at the mountain front ranges from 0.03-0.07% for the Narayani, Karnali, and Kosi rivers (Galy et al., 2008). These rivers account for ~67% of the total sediment flux to the main stem Ganges, and yield a sediment-flux weighted average value of C_{org_petro}=0.05% compared to C_{org_petro}=0.025% on the Ganges near its outlet in Bangladesh (Galy et al., 2008; Galy et al., 2015). Using the flux-weighted average C_{org_petro} value, and assuming the unconstrained tributaries have $0.0<C_{org\_petro}<0.05\%$, yields C_{org_petro} losses of 27-51% from the mountain front to the Ganges in Bangladesh.

In order to compare field measurements with our experiments of ~900-1200 km of suspended sediment transport (Table DR2), we assume POC_{petro} losses are linearly proportional to river transport distance. Based on the ~2300 km of transport between the Rio Beni at Rurrenabaque and the mouth of the Rio Madiera we reduce transport losses by a factor of 1000 km / 2300 km = 0.43 to yield C_{org_petro} losses of 7-41% per 1000 km of fluvial transit in the Amazon basin. Transport distances between the mountain front and the lowland Ganges in Bangladesh range from ~550-1000 km for pathways investigated by Galy et al (2008). As the upper limits of these distances approximately match the transport in our flume experiment, we conservatively apply no correction and estimate POC_{petro} losses of 27-51% per ~500-1000 km of transport in the Ganges basin.

While the field measurements and flume experiments can be compared using similar transport length scales, they represent timescales that can differ by orders of magnitude. By continuously transporting sediment without floodplain storage, our flume experiments achieved order ~1000 km of suspended sediment transport in ~50 days. In contrast, the residence time of sediment crossing the Amazon basin can be of order ky (Dosseto et al., 2006; Wittmann et al., 2015), due to transient floodplain storage during downstream transit. The negligible POC losses observed in our flume experiments compared to the large losses observed in the Amazon and Ganges basins are consistent with the hypothesis that the majority of POC oxidation occurs during floodplain storage (Torres et al., 2017; Scheingross et al., 2018). Trapping of sediment behind natural and man-made dams may provide an additional source of sediment storage; however, high sedimentation rates in dams is thought to promote POC preservation (Li et al., 2015), rather than oxidation which can occur in shallow floodplain deposits.

9. Pilot experiments

We performed three pilot experiments to aid in designing the experimental protocol. Differences in methods and standards between the pilot and main experiments make comparing the experiment sets difficult; nonetheless we report the pilot experiment methods and data for

archival purposes. Two of the pilot experiments used the same lignite and shale sediment from the main experiments, while the third used organic-rich soil collected within 5 cm of the surface from a temperate forest in Potsdam, Germany. We expect that the soil should be free of POC_{petro} due to the combination of high rates of litterfall in the forest and underlying deposits of glacial outwash sands derived largely from Fennoscandian basement rocks

Pilot experiments followed identical methods to the primary experiments discussed in the main text with the exceptions listed here. Pilot experiments used a smaller volume control tank and had different sediment to water ratios than the main experiments (Table DR2). The pilot soil and lignite experiments used exclusively de-ionized water, and the pilot shale experiment used exclusively tap water. In the pilot shale experiment we added fresh sediment to both the flume and control after ~14 days to observe the effect of sediment doubling. In the pilot soil experiment, we dry-sieved 150 g soil to <125 μm and added 50 g of 125-400 μm diameter combusted quartz sand to promote soil comminution. Quartz sand was within the zone of partial viscous damping, limiting its abrasion in the experiment and allowing separation of the quartz and soil at the end of the experiment by sieving to size fractions greater and less than 125 μm, respectively. In pilot experiments with soil and lignite (Table DR2) we progressively added ~2 L of water to the flume over the course of the experiment and ~0.2 – 0.5 L to the control tank to account for evaporative and sample losses.

References:

Bagnold, R. A., 1966, An approach to the sediment transport problem for general physics: Washington, D.C., US Geological Survey Professional Paper 422-I.

Beaupre, S. R., Mahmoudi, N., and Pearson, A., 2016, IsoCaRB: A novel bioreactor system to characterize the lability and natural carbon isotopic (C-14, C-13) signatures of microbially respired organic matter: Limnology and Oceanography-Methods, v. 14, no. 10, p. 668-681.

Bouchez, J., Beyssac, O., Galy, V., Gaillardet, J., France-Lanord, C., Maurice, L., and Moreira-Turcq, P., 2010, Oxidation of petrogenic organic carbon in the Amazon floodplain as a source of atmospheric CO2: Geology, v. 38, no. 3, p. 255-258.

Brunauer, S., Emmett, P., and Teller, E., 1938, Adsorption of Gases in Multimolecular Layers: Journal of the American Chemical Society, v. 60, no. 2, p. 309-319.

Chang, S. B., and Berner, R. A., 1999, Coal weathering and the geochemical carbon cycle: Geochimica Et Cosmochimica Acta, v. 63, no. 19-20, p. 3301-3310.

Chanson, H., 2004, Hydraulics of Open Channel Flow, Amsterdam, Elsevier.

Chatanantavet, P., Whipple, K. X., Adams, M. A., and Lamb, M. P., 2013, Experimental study on coarse grain saltation dynamics in bedrock channels: Journal of Geophysical Research-Earth Surface, v. 118, no. 2, p. 1161-1176.

Chou, L., Garrels, R. M., and Wollast, R., 1989, Comparitive study of the kinetics and mechanisms of dissolution of carbonate minerals: Chemical Geology, v. 78, p. 269-282.

Chu, Z. Y., Yan, Y., Chen, Z., Guo, J. H., Yang, Y. H., Li, C. F., and Zhang, Y. B., 2015, A Comprehensive Method for Precise Determination of Re, Os, Ir, Ru, Pt, Pd Concentrations and Os Isotopic Compositions in Geological Samples: Geostandards and Geoanalytical Research, v. 39, no. 2, p. 151-169.

Dietrich, W. E., 1982, Settling velocity of natural particles: Water Resources Research, v. 18, no. 6, p. 1615-1626.

Dosseto, A., Bourdon, B., Gaillardet, J., Allegre, C. J., and Filizola, N., 2006, Time scale and conditions of weathering under tropical climate: Study of the Amazon basin with U-series: Geochimica Et Cosmochimica Acta, v. 70, no. 1, p. 71-89.

Galy, V., Beyssac, O., France-Lanord, C., and Eglinton, T., 2008, Recycling of Graphite During Himalayan Erosion: A Geological Stabilization of Carbon in the Crust: Science, v. 322, no. 5903, p. 943-945.

Galy, V., Bouchez, J., and France-Lanord, C., 2007, Determination of total organic carbon content and delta C-13 in carbonate-rich detrital sediments: Geostandards and Geoanalytical Research, v. 31, no. 3, p. 199-207.

Galy, V., Peucker-Ehrenbrink, B., and Eglinton, T., 2015, Global carbon export from the terrestrial biosphere controlled by erosion: Nature, v. 521, no. 7551, p. 204-207.

Garcia, M. H., 2008, Sediment transport and morphodynamics, *in* Garcia, M. H., ed., Sedimentation Engineering: Processes, Measurements, Modeling, and Practice: Reston, Virginia, American Society of Civil Engineers.
Grocke, D. R., Hori, R. S., Trabucho-Alexandre, J., Kemp, D. B., and Schwark, L., 2011, An open ocean record of the Toarcian oceanic anoxic event: Solid Earth, v. 2, no. 2, p. 245-257.
Joseph, G. G., Zenit, R., Hunt, M. L., and Rosenwinkel, A. M., 2001, Particle-wall collisions in a viscous fluid: Journal of Fluid Mechanics, v. 433, p. 329-346.
Li, G., Wang, X. C. T., Yang, Z. F., Mao, C. P., West, A. J., and Ji, J. F., 2015, Dam-triggered organic carbon sequestration makes the Changjiang (Yangtze) river basin (China) a significant carbon sink: Journal of Geophysical Research-Biogeosciences, v. 120, no. 1, p. 39-53.
Lupker, M., France-Lanord, C., and Lartiges, B., 2016, Impact of sediment-seawater cation exchange on Himalayan chemical weathering fluxes: Earth Surface Dynamics, v. 4, no. 3, p. 675-684.
McLean, S. R., 1992, On the calculation of suspended-load for noncohesive sediments: Journal of Geophysical Research-Oceans, v. 97, no. C4, p. 5759-5770.
Miller, C. A., Peucker-Ehrenbrink, B., and Ball, L., 2009, Precise determination of rhenium isotope composition by multi-collector inductively-coupled plasma mass spectrometry: Journal of Analytical Atomic Spectrometry, v. 24, no. 8, p. 1069-1078.
Rohl, H. J., Schmid-Rohl, A., Oschmann, W., Frimmel, A., and Schwark, L., 2001, The Posidonia Shale (Lower Toarcian) of SW-Germany: an oxygen-depleted ecosystem controlled by sea level and palaeoclimate (vol 165, pg 27, 2001): Palaeogeography Palaeoclimatology Palaeoecology, v. 169, no. 3-4, p. 271-+.
Sayles, F. L., and Mangelsdorf, P. C., 1979, Cation-Exchange Characteristics of Amazon River Suspended Sediment and Its Reaction with Seawater: Geochimica Et Cosmochimica Acta, v. 43, no. 5, p. 767-779.
Scheingross, J. S., Brun, F., Lo, D. Y., Omerdin, K., and Lamb, M. P., 2014, Experimental evidence for fluvial bedrock incision by suspended and bedload sediment: Geology, v. 42, no. 6, p. 523-526.
Scheingross, J. S., Repasch, M., Hovius, N., Sachse, D., Dellinger, M., Lupker, M., Hilton, R. G., Eglinton, T., Grocke, D., Golombek, N., and Orfeo, O., 2018, The fate of organic carbon during lowland river transport and transient floodplain storage: AGU Fall Meeting abstract V11E-0070.
Schreck, P., and Glasser, W., 1998, Regional geology of the lignite mining districts in eastern Germany: Acidic Mining Lakes, p. 15-21.
Schuessler, J. A., Kampf, H., Koch, U., and Alawi, M., 2016, Earthquake impact on iron isotope signatures recorded in mineral spring water: Journal of Geophysical Research-Solid Earth, v. 121, no. 12, p. 8548-8568.
Sklar, L. S., and Dietrich, W. E., 2004, A mechanistic model for river incision into bedrock by saltating bed load: Water Resources Research, v. 40, no. 6.
Smith, J. C., 2013, Particulate organic carbon mobilisation and export from temperate forested uplands [PhD: University of Cambridge.
Torres, M. A., Limaye, A. B., Ganti, V., Lamb, M. P., West, A. J., and Fischer, W. W., 2017, Model predictions of long-lived storage of organic carbon in river deposits: Earth Surface Dynamics, v. 5, no. 4, p. 711-730.
White, A. F., and Brantley, S. L., 2003, The effect of time on the weathering of silicate minerals: why do weathering rates differ in the laboratory and field?: Chemical Geology, v. 202, no. 3-4, p. 479-506.
Wittmann, H., von Blanckenburg, F., Dannhaus, N., Bouchez, J., Gaillardet, J., Guyot, J. L., Maurice, L., Roig, H., Filizola, N., and Christl, M., 2015, A test of the cosmogenic Be-10(meteoric)/Be-9 proxy for simultaneously determining basin- wide erosion rates, denudation rates, and the degree of weathering in the Amazon basin: Journal of Geophysical Research-Earth Surface, v. 120, no. 12, p. 2498-2528.

Data Repository Tables (see separate excel file)

Table DR1: Flow velocity measurements
Table DR2: Summary of experiments
Table DR3: Summary of solid load carbon, rhenium, and granulometry measurements
Table DR4: Results of liquid-chromatography organic carbon detection (LC-OCD) measurements
Table DR5: Multiprobe measurements of flume and control tank water
Table DR6: Inorganic dissolved load measurements
Table DR7: Uncertainty estimates of dissolved load measurements

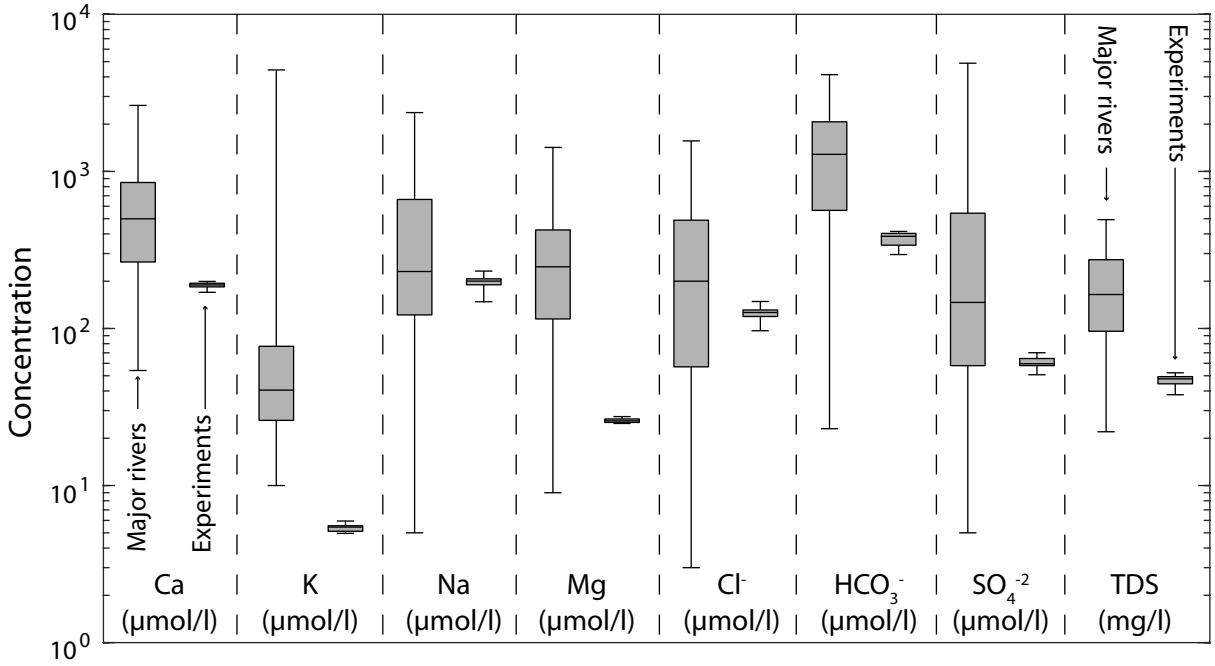

Figure DR1: Comparison of dissolved chemistry from major rivers (Gaillardet et al., 1999) (left box plots) versus starting composition of water used in experiments (right box plots). Box and whisker plots show data median, interquartile range, and data extent. Following Gaillardet et al. (1999), we excluded rivers with total dissolved solids (TDS) >500 mg/l based on likely anthropogenic influence.

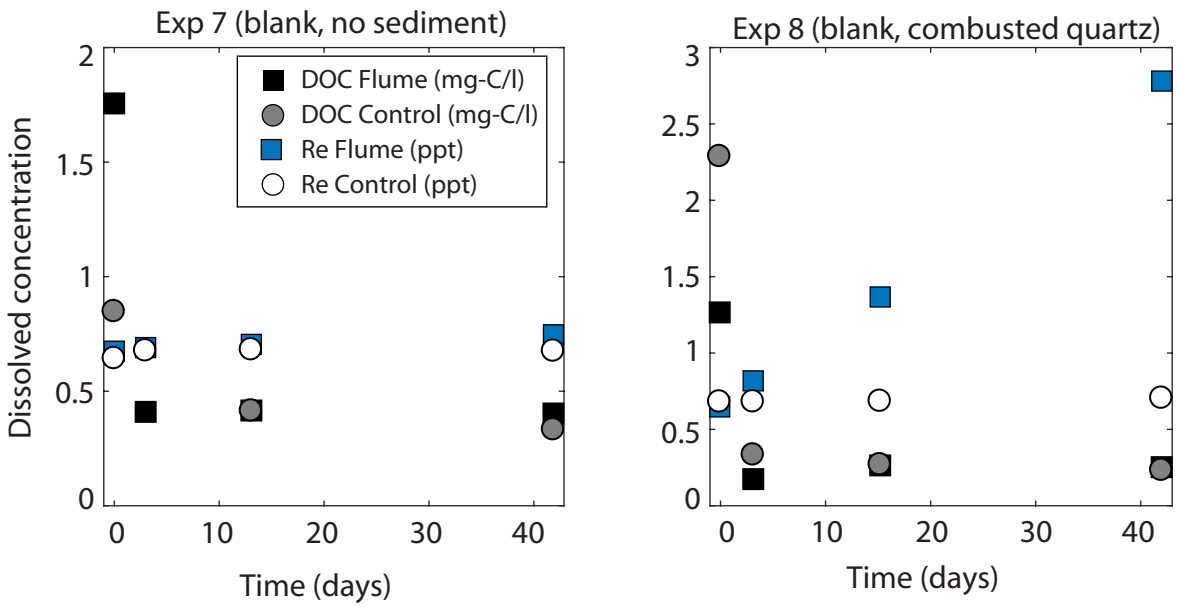

Figure DR2: Evolution of dissolved organic carbon (DOC) and Re concentrations in blank experiments.

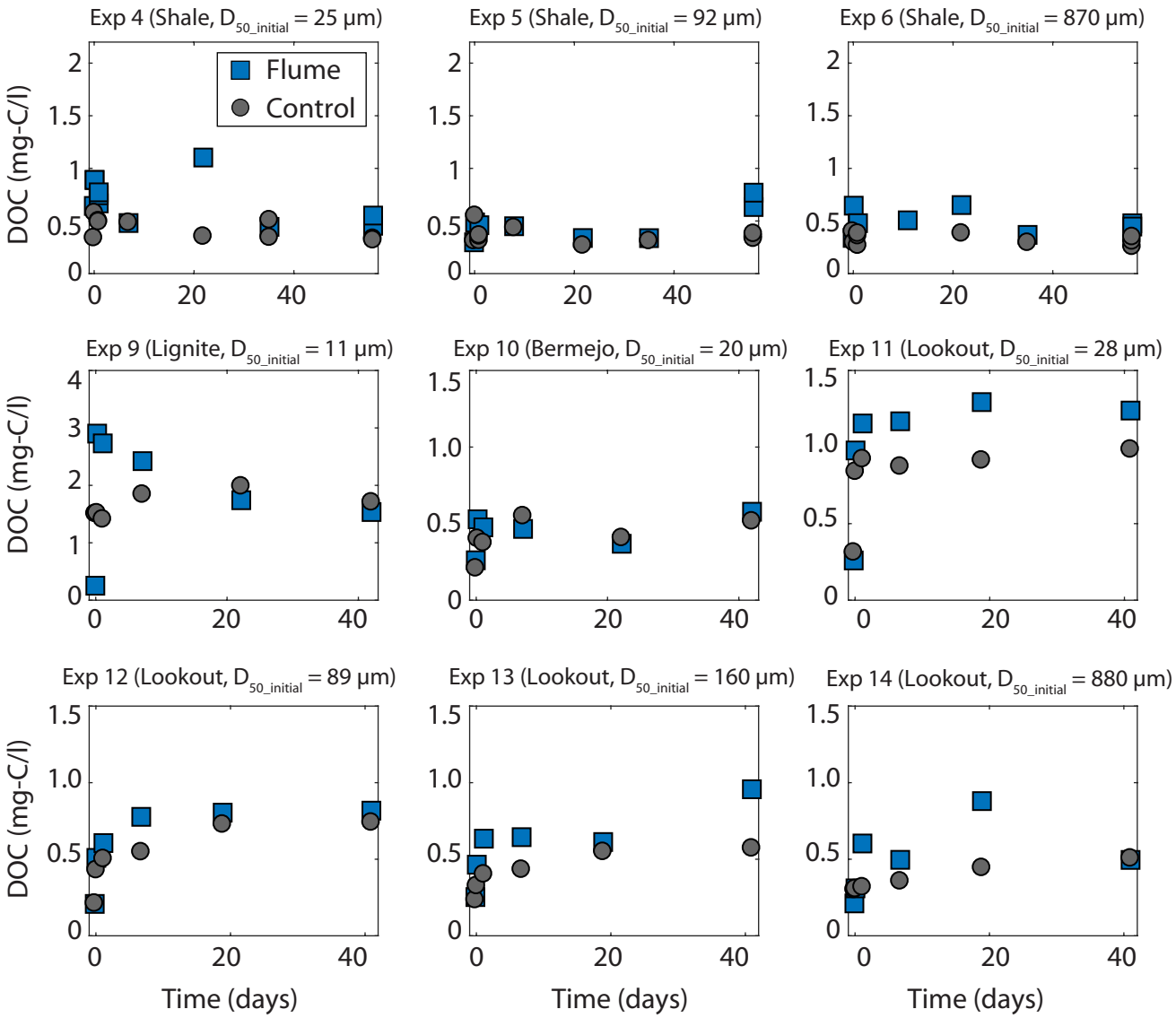

Figure DR3: Evolution of dissolved organic carbon (DOC) concentration during flume and control experiments. $D_{50\_initial}$ is the median grain diameter at the start of the experiment.

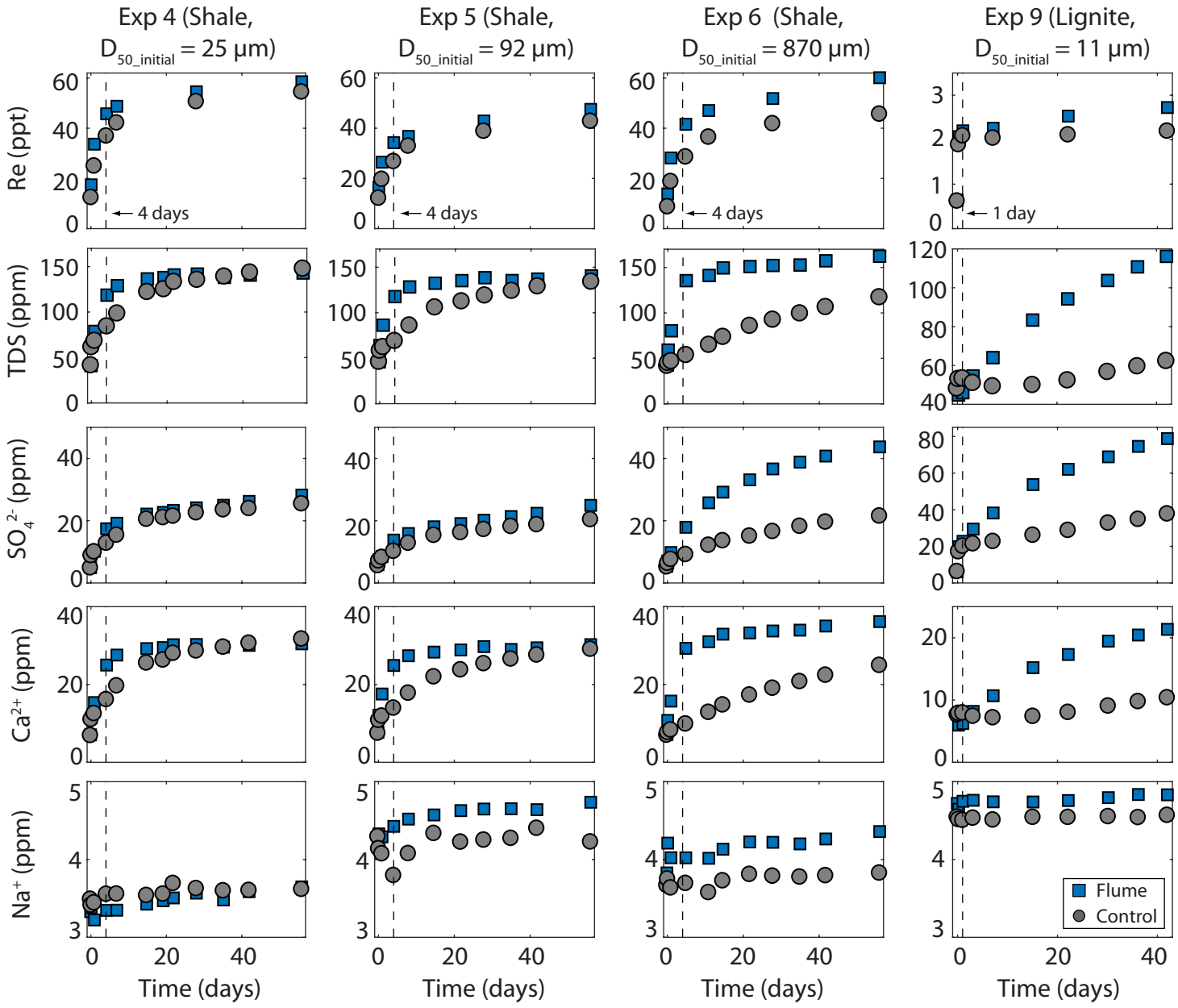

Figure DR4: Evolution of dissolved rhenium, total dissolved solids (TDS), SO_4^{2-}, Ca^{2+}, and Na^+ for POC_{petro} experiments. Dashed lines show the transition from rapid solute production inconsistent with lowland rivers to inferred oxidative weathering. $D_{50\_initial}$ is the grain diameter at the start of the experiment.

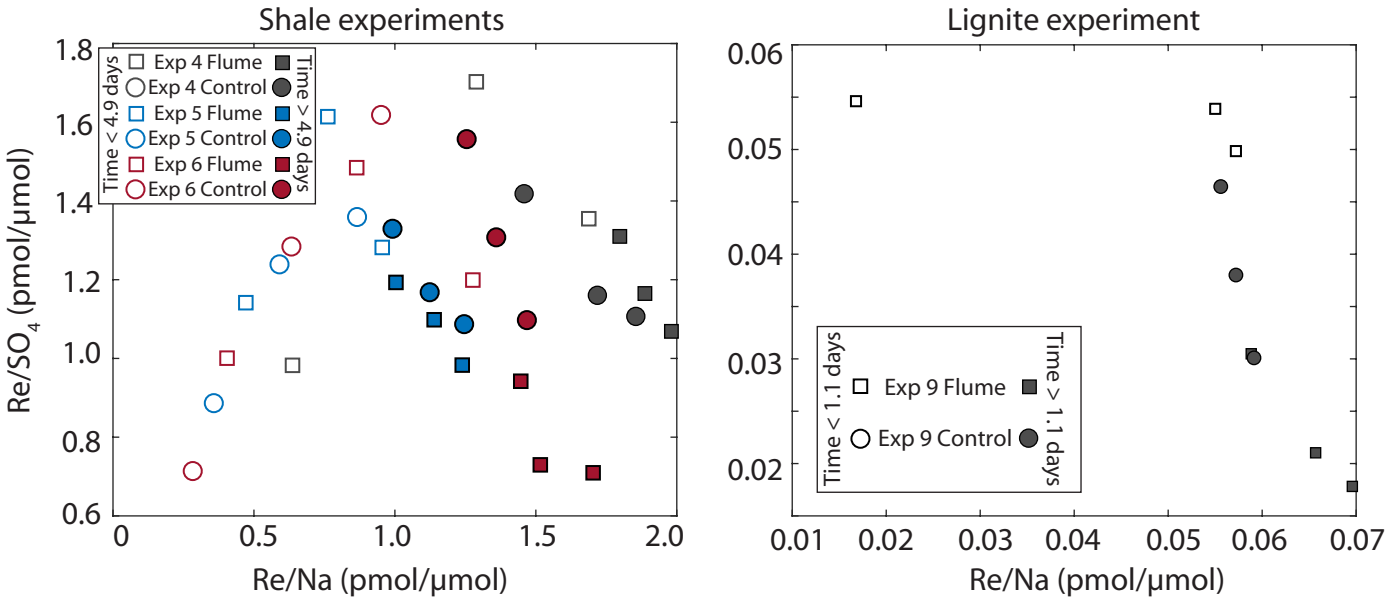

Figure DR5: Re/SO_4 vs Re/Na for shale and lignite experiments. Open symbols are periods of rapid solute production and closed symbols are periods of inferred oxidative weathering.